

Enhancement of the conversion efficiency of selective emitter PERC solar cells by post-oxidation

Rui Tong^a, Hui Zheng^a, Sheng Ma^b, Dongming Liu^{a,*}, Changtong Xu^c, Weipeng Zhang^c, Xiaofeng Liu^d

^a School of Materials Science and Engineering, Anhui University of Technology, Maanshan, Anhui, 243002, China

^b School of Materials Science and Engineering, Shanghai Jiao Tong University, Shanghai, 200240, China

^c Nantong Sumin Renewable Energy Technology Co., Ltd, Nantong, Jiangsu, 226333, China

^d School of Material Science and Engineering, Zhejiang University, Hangzhou, Zhejiang, 310027, China



ARTICLE INFO

Keywords:

Solar cell
Post-oxidation
Laser-induced damage
Oxide layer
Efficiency

ABSTRACT

Thermal oxidation has been widely adopted in the fabrication process of silicon solar cells. In this paper, we investigate the effect of thermal oxidation on the performance of passivated emitter and rear cells (PERC) after the diffusion process. It is found that the application of a diffusion furnace for post-oxidation results in the re-doping of phosphorus, which affects the minority carrier lifetime and implied V_{oc} . In comparison, the use of an annealing furnace for post-oxidation brings an improvement of electrical properties of solar cells because of the gettering effect. Furthermore, the increase in thickness of the oxide layer mitigates the laser-induced damage during the laser doping process, which is beneficial for the enhancement of cell efficiency. Batch data shows that post-oxidation using an annealing furnace leads to an absolute efficiency improvement by 0.1%.

1. Introduction

Recent years have witnessed a steady improvement in the conversion efficiency of crystalline silicon (Si) solar cells due to the continuous technical improvement of manufacturing techniques [1–4]. Owing to the low-cost manufacturing and high conversion efficiency, the passivated emitter and rear cells (PERC) has dominated the global market [5, 6]. To further improve the conversion efficiency, the selective emitter (SE) technology has been applied for PERC solar cells in past years. The mechanism is that the area with a high doping concentration of phosphorus (P) has a low contact resistance, while the area with a low P-doping concentration effectively reduces the rate of surface recombination [7,8]. In industry, the SE technology has been used in commercial production including laser-doped selective emitter (LDSE) [9,10], ion implantation [11,12] and etching back method [13,14]. Among these technologies, the LDSE technology has been widely used in the production of PERC cells due to its simplicity and low cost.

The LDSE technology was first proposed by Wenham et al. [15]. After continuous development in recent years, the phosphorous silicate glass (PSG) layer has been used as the main source of P in the current industrialized LDSE technology [16]. PSG is mainly composed of SiO_2

and P_2O_5 , and its composition is determined by diffusion temperature, time and gas flow [17,18]. Laser ablation is used to form localized melting on the surface of Si wafer. Since the diffusion coefficient of P in liquid-phase Si is higher than that in solid-phase Si, a higher concentration of P-doping is formed in the ablation area [10], leading to the reduction of sheet resistance of this area. In the subsequent process of the front electrode printing, silver paste is printed in this laser-doped region, thereby reducing the contact resistance by forming a good ohmic contact. However, the localized high temperature heating and rapid cooling of Si during the laser doping process may introduce damages to the substrate such as dislocations, plastic deformation and other crystallographic defects [9]. Hallam et al. found that a low laser doping speed results in the reduction of minority carrier lifetime and the formation of voids [15]. Kim et al. observed the formation of an amorphous Si layer with a thickness of ~10 nm in the laser-doped region, which strongly affects the contact between the front Ag electrode and the selective emitter [19]. Heinrich et al. studied the relationship between the laser-induced damage to Si wafer and picosecond pulse laser wavelength (1064 nm, 532 nm and 355 nm), and pointed out that the three wavelengths of laser all can cause the recrystallization and amorphization of the crystalline Si structure [20]. Fellmeth et al. found

* Corresponding author.

E-mail address: ldm1975@ahut.edu.cn (D. Liu).

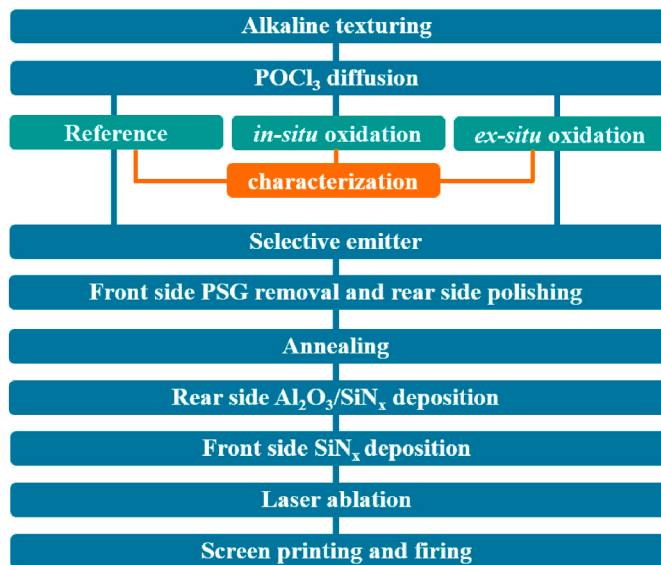


Fig. 1. Process flow for the fabrication of the solar cells.

that the sheet resistance reduced to $31 \Omega/\square$ after laser doping of a Si wafer with a diffusion resistance of $110 \Omega/\square$, and the corresponding emitter saturation current density (J_{0e}) increased from 264 to 575 fA/cm^2 and open-circuit voltage (V_{oc}) limit decreased from 658 to 637 mV [21]. Therefore, reducing the laser-induced damage and influence to Si wafer has an important impact on further improving the conversion efficiency of solar cells.

On the other hand, thermal oxidation process has been widely used in the production of solar cells. For monocrystalline Si cells, the processing of rapid thermal oxidation (RTO) had been applied to attain surface recombination velocity value approaching 10 cm/s on the $1.25 \Omega \text{ cm}$ p-type Si wafer [22], and the conversion efficiency was enhanced by 0.23% [23]. In the presence of a SiO_2 layer grown by thermal oxidation between the Si substrate and the SiN_x layer, the number of surface dangling bonds could be reduced and the performance of solar cells could be improved [24]. In the production process of tunnel oxide passivated contact (TOPCon) solar cell, the ultra-thin tunnel oxide layer could be grown by the thermal oxidation method [25,26]. Hence, it is of great significance to analyze the interaction between the laser SE process and thermal oxidation process performed after the diffusion process, which would be helpful in unraveling the impact on the performance of SE PERC solar cells.

In this work, post-oxidation was carried out on the samples by diffusion furnace and annealing furnace after the diffusion process, respectively, and the impact on samples' performance was studied. Furthermore, the relationship between the oxide layer grown by annealing furnace and the laser-induced damage to the sample was analyzed and the mechanism of how the oxide layer mitigates the laser-induced damage was also revealed. By using the optimized post-oxidation process, we fabricated the solar cell with a higher conversion efficiency than that of the reference group by 0.1%.

2. Experimental

A batch of boron-doped p-type monocrystalline Si wafers ($158.75 \text{ mm} \times 158.75 \text{ mm}$) with a resistivity range of $1.2\text{--}1.3 \Omega \text{ cm}$ and a thickness of $180 \mu\text{m}$ were used in this work. The samples were textured by the traditional alkaline texturing process and cleaned by HF/HCl mixed solution and deionized water. The low-pressure diffusion process was adopted and the process sequence was set as deposition-drive-in-deposition. After the diffusion process, the diffusion furnace and annealing furnace were used for the post-oxidation process. Then the

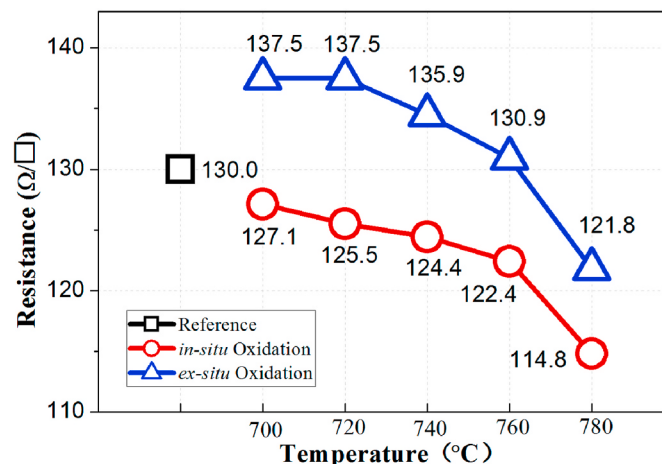


Fig. 2. Correlation between post-oxidation temperature and sheet resistance.

laser-doped selective emitter, acid etching, annealing, rear side $\text{Al}_2\text{O}_3/\text{SiNx}$ stack coating, front side SiN_x layer coating, rear side laser ablation, printing and sintering processes were implemented. The detailed process flow was shown in Fig. 1.

The laser-induced damage area was observed by a Hitachi SU3500 scanning electron microscope (SEM). The concentration of P atoms and diffusion profile in the sample were evaluated by a WEP CVP21 electrochemical capacitance-voltage profiler (ECV). The sheet resistance was measured by the four-probe method (RG-200PV*DF-9P, Napson) and the thickness of the oxide layer was characterized by an ellipsometer (COSE PV 4.1, Syscos). A Sinton WCT-120 system was used to measure the minority carrier lifetime and implied V_{oc} . Finally, a Halm cetisPV-IUCT-2400 I-V tester was applied to measure the electrical parameters of solar cells under AM1.5G.

3. Results and discussion

3.1. Comparison of in-situ and ex-situ oxidation

In the production of PERC solar cells, oxygen atmosphere is used in the diffusion process and annealing process [24,27]. Therefore, in this work, post-oxidation was carried out by a diffusion furnace for *in-situ* oxidation and an annealing furnace for *ex-situ* oxidation by taking out the wafers from the diffusion furnace, respectively. The temperatures were set to 700°C , 720°C , 740°C , 760°C and 780°C . The flow rate of oxygen was set to 1000 sccm , and the post-oxidation time was set to 20 min. As reported previously [18], the introduction of oxygen during the diffusion process results in the formation of PSG and SiO_2 layers with different thicknesses depending on the process time. The upper layer is PSG film and the bottom layer is SiO_2 film. In this paper, we do not make a further distinction between these two layers, and refer them as an oxide layer.

The sheet resistance was measured under different temperatures, and the results are shown in Fig. 2. It can be seen that as the temperature increases from 700 to 780°C , the sheet resistance of the two groups of samples shows a clear decrease. In addition, the values of all samples after post-oxidation in the diffusion furnace are lower than that of the reference group. After the samples were subjected to post-oxidation in the annealing furnace, the sheet resistances of the samples are higher than that of the reference group at $700\text{--}760^\circ\text{C}$ and lower when the temperature is higher than 760°C . The sheet resistance is reduced for samples with a higher surface doping concentration and a deeper diffusion junction [7,28,29].

To further understand these results, a mechanistic illustration is presented in Fig. 3, which differentiates the pristine sample (reference) from the samples after post-oxidation at different temperatures. For *in-*

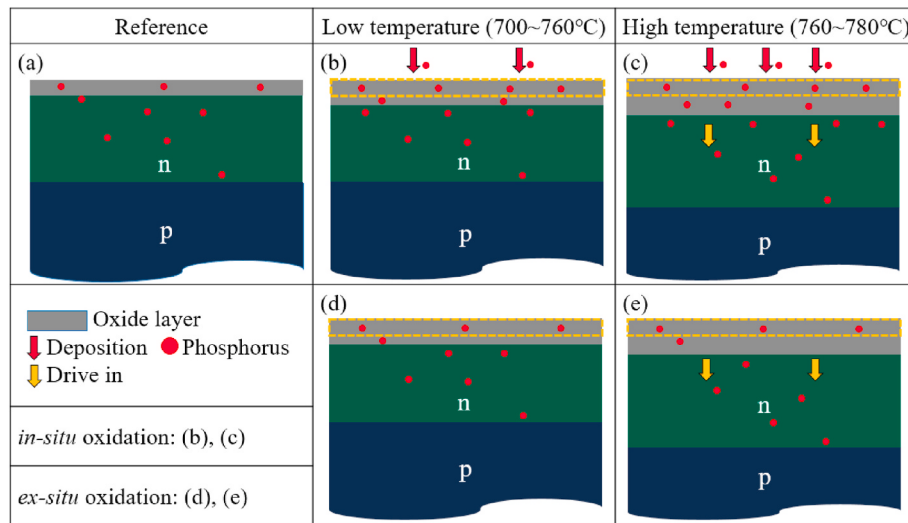


Fig. 3. Schematic diagrams for illustrating the effect of oxidation process on P diffusion.

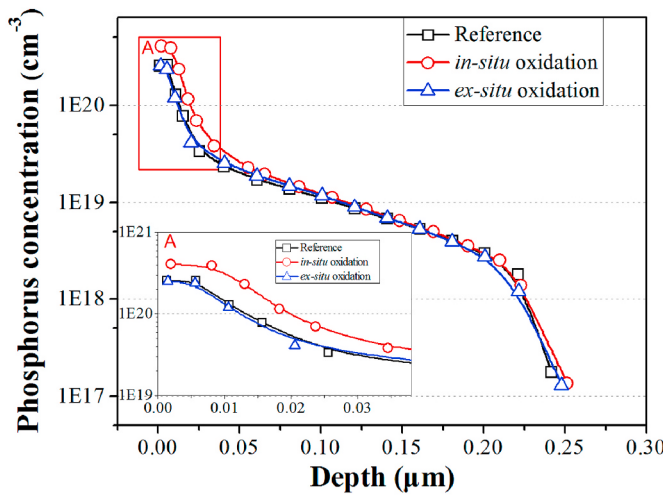


Fig. 4. The influence of different post-oxidation methods on ECV profile.

situ oxidation, due to the presence of residual P in the furnace tube, the surface of Si wafer becomes P-doping again during the post-oxidation step, which increases the doping concentration of wafer surface and leads to the reduction in the sheet resistance (Fig. 3b and c). For *ex-situ* oxidation at temperatures lower than 760 °C, the increase in thickness of the oxide layer reduces the active P concentration of Si surface (Fig. 3d).

As the oxidation temperatures higher than 760 °C, P atoms could diffuse from the surface into the Si substrate and increase the depth of p-n junction, thus resulting in the reduction in resistance (Fig. 3e).

As indicated above, a higher oxidation temperature is connected to a larger diffusion length of P and could affect the surface doping concentration. In order to verify this hypothesis, the lower oxidation temperature of 700 °C was chosen to examine the potential difference in the surface doping concentration of the two groups of samples. Fig. 4 gives the ECV profiles of samples after the *in-situ* and *ex-situ* oxidation processes at 700 °C. The difference in surface P concentration is large, while the junction depths are similar. For *in-situ* oxidation, the surface doping concentration is about $3.9 \times 10^{20} \text{ cm}^{-3}$, as compared to $2.6 \times 10^{20} \text{ cm}^{-3}$ for *ex-situ* oxidation. This difference is mainly due to the residual P in the furnace tube during *in-situ* oxidation.

To study the influence of the two post-oxidation methods on the sample performance, the samples were divided into three groups: the reference group without oxidation and the two groups with *in-situ* and *ex-situ* oxidation. All samples were polished on both sides by HF/HNO₃/H₂O mixed acid solution to remove the damage layer. After being rinsed with DI water, the P was diffused on both sides of samples. For the two oxidation groups, the oxidation temperature, oxygen flow and oxidation time were set as 700 °C, 1000 sccm and 20 min, respectively. After post-oxidation, the PSG layers of all samples were removed and double-side SiN_x deposition was performed. Then the rapid thermal process (RTP) was carried out [30] and the minority carrier lifetime and implied V_{oc} were measured. Fig. 5 shows the minority carrier lifetime at an injection level of $1 \cdot 10^{15}/\text{cm}^3$ and the implied V_{oc} at one-sun illumination intensity

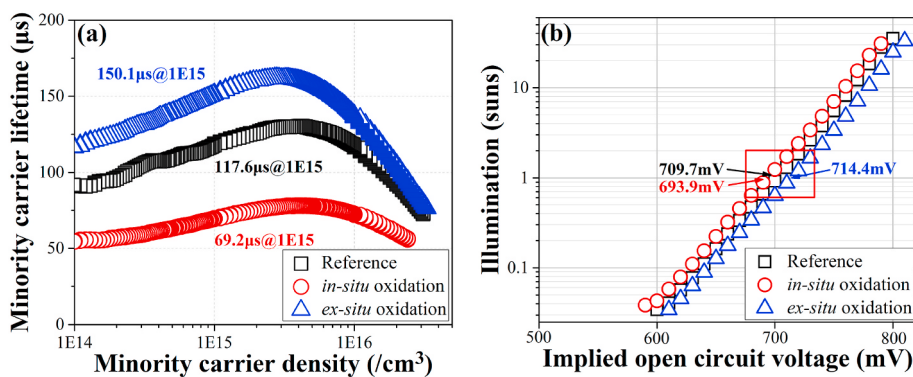


Fig. 5. (a) Minority carrier lifetime as a function of injection level and (b) implied V_{oc} as a function of illumination for the samples after different post-oxidation treatments at 700 °C.

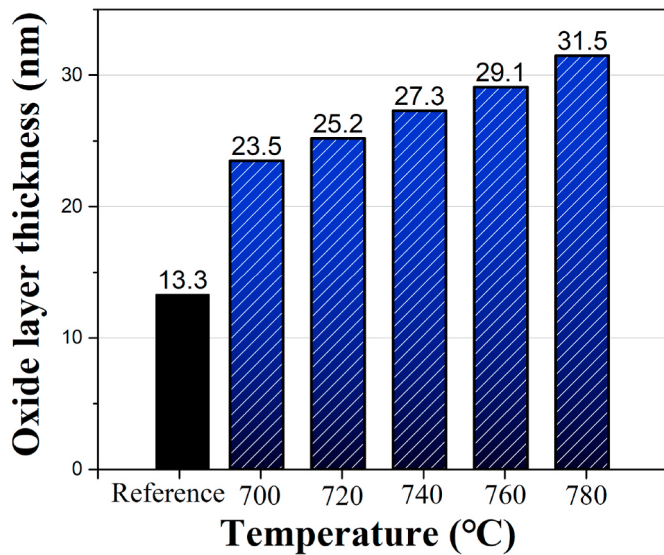


Fig. 6. The influence of oxidation temperature on the thickness of oxide layer.

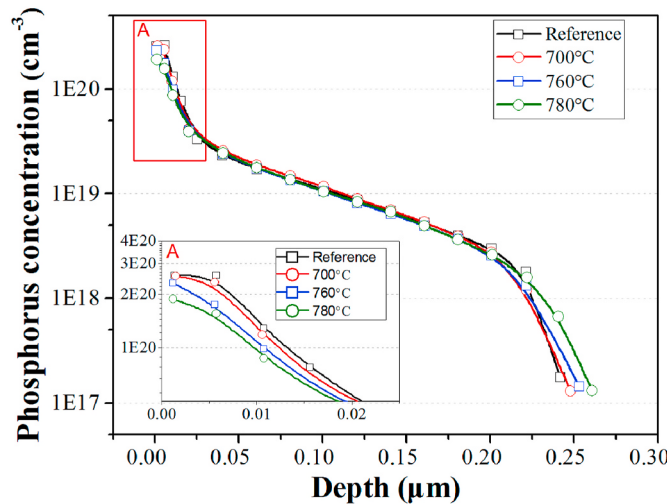


Fig. 7. The depth profile of P doping concentration for samples at different temperatures.

of the three groups. It can be seen that the lifetimes of reference, *in-situ* oxidation and *ex-situ* oxidation groups are 117.6, 69.2 and 150.1 μ s, corresponding to implied V_{oc} of 709.7, 693.9 and 714.4 mV, respectively. The variation rule of minority lifetime is consistent with that of

implied V_{oc} . Due to the introduction of additional P doping during the *in-situ* oxidation, the concentration of inactive P atoms on the surface are significantly increased. Thus the surface Shockley-Read-Hall (SRH) recombination is increased [31], resulting in the reduction of minority carrier lifetime and implied V_{oc} . In comparison, for *ex-situ* oxidation using an annealing furnace, the relatively large segregation coefficient between the bulk Si and P-doped surface may result in P gettering [32], which can reduce the surface doping concentration as the oxide layer is removed in the following process. Thus the minority carrier lifetime and implied V_{oc} are both enhanced.

3.2. The effect of temperature on oxide layer thickness and ECV profiles

Based on the above analysis, the *ex-situ* oxidation method was chosen as the post-oxidation process in the following experiments. To examine the temperature dependence, we first measured the thickness of oxide layer for the reference without post-oxidation and the samples oxidized at 700 °C, 720 °C, 740 °C, 760 and 780 °C. As shown in Fig. 6, the thickness of oxide layer formed during the diffusion process for the reference sample is 13.3 nm. With the oxidation temperature increases from 700 to 780 °C, the oxide layer thickness increases from 23.5 to 31.5 nm for the oxidation samples. In addition, since the sheet resistance starts to decrease significantly for samples oxidized at 760 °C, we further compared the difference in diffusion concentration and ECV profiles for samples oxidized at 700 °C, 760 °C and 780 °C. It can be seen from Fig. 7 that the surface P concentration and junction depth of the sample oxidized at 700 °C changes slightly in comparison with the reference sample. For the sample oxidized at 760 °C, the surface doping concentration is reduced, and the diffusion junction depth becomes larger. This tendency is more obvious for the sample oxidized at 780 °C. The result suggests that the diffusion of P into the Si substrate leads to an increase in junction depth at 760 °C, which is also responsible for the decrease in sheet resistance under the present experimental conditions.

3.3. The impact of oxide layer on laser-induced damage

Since the change of surface doping concentration could affect the series resistance (R_s) and a high temperature is easy to bring undesirable diffusion-related and temperature-sensitive effects [23], a lower-temperature oxidation process is favorable in our experiment. Therefore, in order to reduce the influence of such variable factors, and keep the diffusion concentration and junction depth close to that of the reference group, *ex-situ* oxidation at 700 °C was carried out to analyze the impact of laser-induced damage on the performance of solar cells. Additionally, the sample without oxidation treatment was used as the reference group.

As shown in Fig. 8, after SE process, the sheet resistances of SE region are reduced from 130.0 to 71.2 Ω/\square and 137.5 to 83.3 Ω/\square , with the reduction ratios of 45.2% and 39.4% for the reference and experimental groups, respectively. Furthermore, the ECV profile shows that the

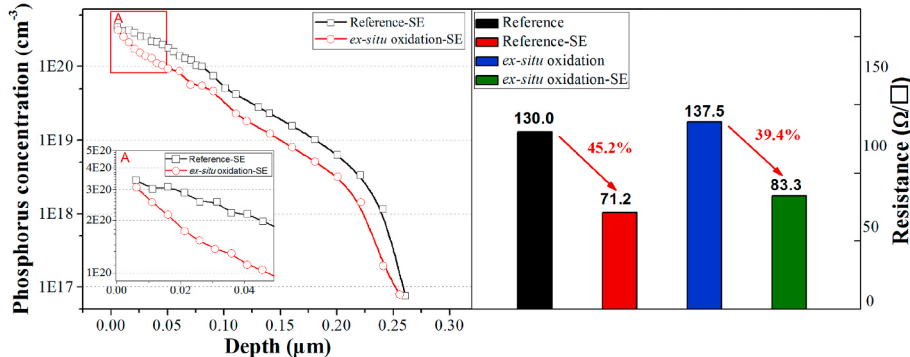


Fig. 8. ECV profiles of SE region and resistance change before and after SE.

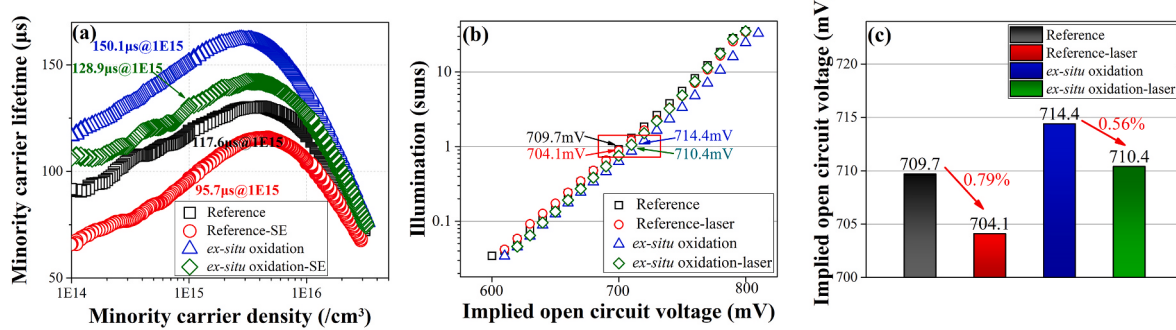


Fig. 9. Influence of *ex-situ* oxidation treatment at 700 °C and laser-induced damage on (a) minority carrier lifetime and (b,c) implied V_{oc} .

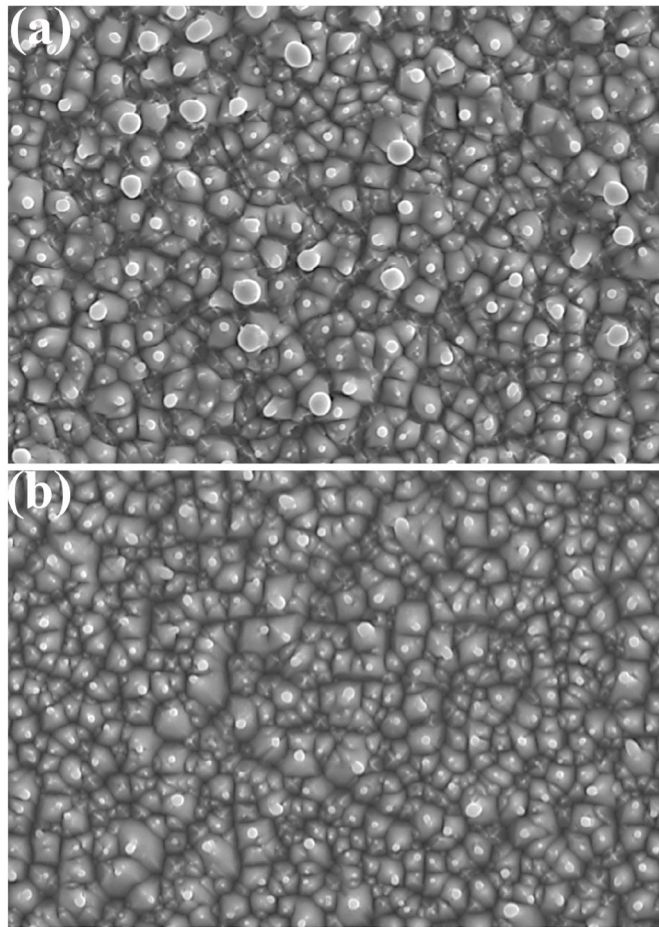


Fig. 10. SEM images for the surfaces of laser-doped wafers: (a) reference group without oxidation, (b) after *ex-situ* oxidation at 700 °C.

overall concentration of the experimental group is lower than that of the reference group. This result can be attributed to the presence of the thicker oxide layer that blocks the laser ablation of Si, reducing the heat absorption of the Si substrate and slowing down the diffusion of P atoms in Si.

To further study the influence of oxide layer thickness on the solar cell performance, an additional laser doping process was performed on one side of the reference group after diffusion process and the experimental group with *ex-situ* oxidation process. The area for laser doping is 50 mm × 50 mm. The minority carrier lifetime and implied V_{oc} of the four groups are compared in Fig. 9, where the samples processed by laser doping were denoted as the reference-laser and *ex-situ* oxidation-laser. For the sample without post-oxidation treatment, the minority carrier

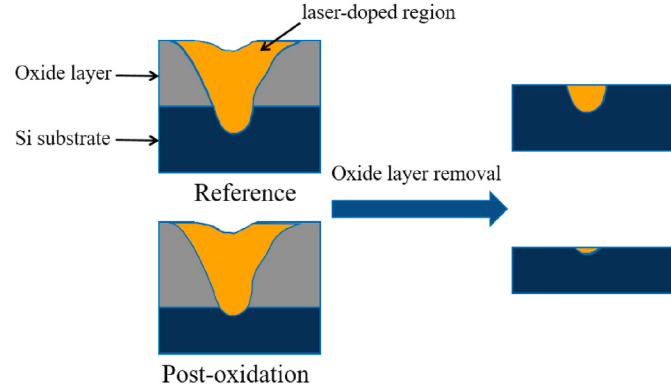


Fig. 11. The mechanism for mitigating of laser-induced damage by the oxide layer on the wafer surface.

lifetime dropped from 117.6 to 95.7 μs and the implied V_{oc} decreased from 709.7 to 704.1 mV by 0.79% after the laser doping process. In comparison, for the sample treated with post-oxidation, the minority carrier lifetime reduced from 150.1 to 128.9 μs and the implied V_{oc} decreased from 714.4 to 710.4 mV by 0.56%. This difference in the reduction of implied V_{oc} suggests that a thicker oxide layer is favorable for mitigating the laser-induced damage of the samples.

Fig. 10 shows the SEM images for the surface morphology of the wafer samples after SE process. White dots with varying sizes are observed on the top of the pyramids of the sample surface, implying partial melting of the pyramidal surface structures [19]. Larger structural changes in the surface of the pyramids are observed in the experimental group compared with the reference group, which can be explained by the thicker oxide layer that mitigates the laser-induced damage to the Si wafer. Since the thermal conductivity of SiO_2 is lower than that of Si by approximately two orders of magnitude [33–35], the oxide layer blocks the further propagation of heat into the Si wafer and reduces the damage. In addition, the oxide layer can be removed by etching with the $\text{HF}/\text{HNO}_3/\text{H}_2\text{O}$ mixed solution in the subsequent etching process, such that the damaged part of the oxide layer does not affect the performance of the solar cell. Therefore, a thicker oxide layer better protects the Si wafer from laser-induced damage. The removal of the oxide layer reduces the impact of the damage on the performance of solar cells, as schematically explained from Fig. 11.

3.4. Enhancement of electrical performance by *ex-situ* oxidation

A batch of samples was treated by the *ex-situ* oxidation process to verify its influence on the conversion efficiency, and the electrical parameters are shown in Fig. 12. Compared with the reference group, both the V_{oc} and short circuit current (I_{sc}) are increased. This is because the

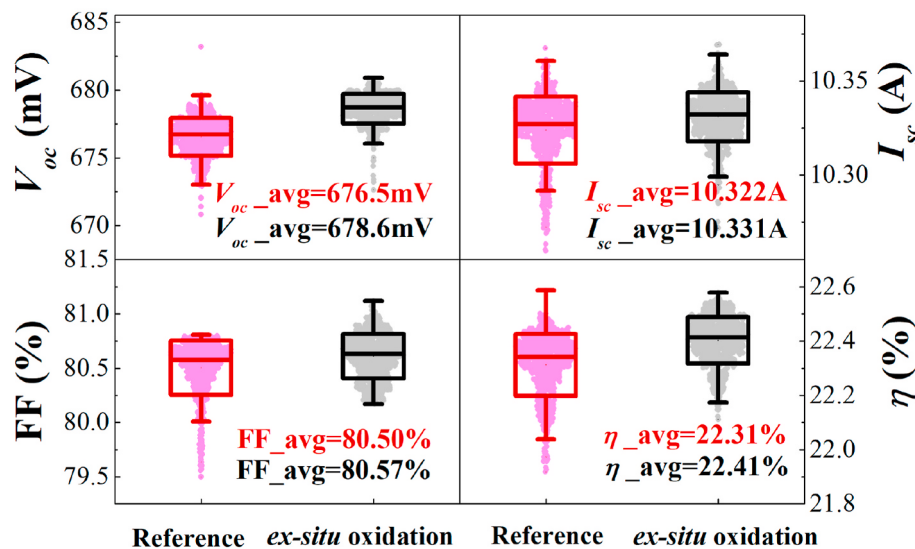


Fig. 12. Comparison of electrical parameters for the cell samples with and without *ex-situ* oxidation process.

ex-situ oxidation process improves the minority carrier lifetime of solar cells and the thicker oxide layer reduces the laser-induced damage to the samples. In addition, compared with the reference group, the difference in surface doping concentration and diffusion depth of the oxidized samples after SE is related with an increase in sheet resistance ($71.2 \Omega/\square$ for the reference group and $83.3 \Omega/\square$ for the experimental group), which could lead to an increase in R_s and reduction in fill factor (FF) [7, 36]. However, in the present case, the decrease of FF is not observed possibly due to the positive benefits offered by the reduction of the surface and internal defects [37,38]. Due to the change in electrical performance, the average efficiency (η) of solar cells increases from 22.31% to 22.41%.

4. Conclusions

We have studied the effects of two different post-oxidation processes on the performance of solar cells. The results indicate that the performance of samples processed by *ex-situ* oxidation is better than that processed by *in-situ* oxidation. This is because the residual P in the diffusion furnace tube diffused into the sample and affected the surface P concentration and junction depth. For the *ex-situ* oxidation process, the effect of oxidation temperatures on the thickness of oxide layer was also examined. It was found that the thickness almost increases linearly with the rise of temperature base on the experimental observations. We also proposed a mechanism for the mitigation of laser-induced damage by changing the thickness of the oxide layer formed at 700°C . Finally, a batch of SE PERC solar cells was produced using the *ex-situ* oxidation process. Compared with the reference group, we observed a clear increase in V_{oc} and I_{sc} , and the average efficiency of the samples processed by the *ex-situ* oxidation was higher than that of the reference group by 0.1%.

CRediT authorship contribution statement

Rui Tong: Writing – original draft, Investigation, Data curation, Conceptualization. **Hui Zheng:** Writing – review & editing, Data curation. **Sheng Ma:** Visualization, Data curation. **Dongming Liu:** Writing – review & editing, Supervision, Conceptualization. **Changtong Xu:** Data curation. **Weipeng Zhang:** Visualization, Software, Data curation. **Xiaofeng Liu:** Writing – review & editing, Methodology.

Declaration of competing interest

The authors declare that they have no known competing financial interests or personal relationships that could have appeared to influence the work reported in this paper.

Data availability

Data will be made available on request.

References

- [1] F. Ye, W.W. Deng, W.W. Guo, R.M. Liu, D.M. Chen, Y.F. Chen, et al., 22.13% Efficient industrial p-type mono PERC solar cell, in: Proceedings of the 43rd IEEE PV Specialists Conference, 2016, pp. 3360–3365, <https://doi.org/10.1109/PVSC.2016.7750289>.
- [2] B. Min, M. Muller, H. Wagner, G. Fischer, R. Brendel, P.P. Altermatt, et al., A roadmap toward 24% efficient PERC solar cells in industrial mass production, *IEEE J. Photovoltaics* 7 (2017) 1541–1550, <https://doi.org/10.1109/JPHOTOV.2017.2749007>.
- [3] F. Ye, Y. Li, X. Jia, H. Guo, X. Wang, J. Ding, et al., Optimization of phosphorus dopant profile of industrial p-type mono PERC solar cells, *Sol. Energy Mater. Sol. Cells* 190 (2019) 30–36, <https://doi.org/10.1016/j.solmat.2018.10.002>.
- [4] S. Ma, H.B. Tang, Z.P. Li, X.Y. Kong, W.Z. Shen, Application of SiO_xN_y films in industrial bifacial PERC solar cells, *Sol. Energy Mater. Sol. Cells* 230 (2021), 111199, <https://doi.org/10.1016/j.solmat.2021.111199>.
- [5] D. Zhang, L. Wang, R. Jia, K. Tao, S. Jiang, H. Ge, et al., Improving the performance of PERC silicon solar cells by optimizing the surface inverted pyramid structure on large-area mono-crystalline silicon wafers, *Mater. Sci. Semicond. Process.* 138 (2022), 106281, <https://doi.org/10.1016/j.mssp.2021.106281>.
- [6] Y. Lv, Y.F. Zhuang, W.J. Wang, W.W. Wei, J. Sheng, S. Zhang, et al., Towards high-efficiency industrial p-type mono-like Si PERC solar cells, *Sol. Energy Mater. Sol. Cells* 204 (2020), 110202, <https://doi.org/10.1016/j.solmat.2019.110202>.
- [7] A. Safiei, H. Windgassen, K. Wolter, H. Kurza, Emitter profile tailoring to contact homogeneous high sheet resistance emitter, *Energy Proc.* 27 (2012) 432–437, <https://doi.org/10.1016/j.egypro.2012.07.089>.
- [8] M. Kim, D. Kim, D. Kim, Y. Kang, Laser etch back process to fabricate highly efficient selective emitter c-Si solar cells, *Sol. Energy* 109 (2014) 105–110, <https://doi.org/10.1016/j.solener.2014.08.022>.
- [9] S. Wang, L. Mai, A. Ciesla, Z. Hameiri, D. Payne, C. Chan, et al., Advanced passivation of laser-doped and grooved solar cells, *Sol. Energy Mater. Sol. Cells* 193 (2019) 403–410, <https://doi.org/10.1016/j.solmat.2019.01.025>.
- [10] B. Paviet-Salomon, S. Gall, R. Monna, S. Manuel, A. Slaoui, Experimental and analytical study of saturation current density of laser-doped phosphorus emitters for silicon solar cells, *Sol. Energy Mater. Sol. Cells* 95 (2011) 2536–2539, <https://doi.org/10.1016/j.solmat.2011.03.001>.
- [11] M. Jeon, J. Lee, S. Kim, W. Lee, E. Cho, Ion implanted crystalline silicon solar cells with blanket and selective emitter, *Mater. Sci. Eng. B* 176 (2011) 1285–1290, <https://doi.org/10.1016/j.mseb.2011.07.024>.
- [12] R. Müller, J. Benick, N. Bateman, J. Schön, C. Reichel, A. Richter, et al., Evaluation of implantation annealing for highly-doped selective boron emitters suitable for screen-printed contacts, *Sol. Energy Mater. Sol. Cells* 120 (2013) 431–435, <https://doi.org/10.1016/j.solmat.2013.06.040>.

- [13] Z. Liang, F. Zeng, H. Song, H. Shen, Effect of porous Si and an etch-back process on the performance of a selective emitter solar cell, *Sol. Energy Mater. Sol. Cells* 109 (2013) 26–32, <https://doi.org/10.1016/j.solmat.2012.10.009>.
- [14] C. Kim, J. Lee, S. Lim, C. Jeong, Enhanced absorption and short circuit current density of selective emitter solar cell using double textured structure, *Sol. Energy* 116 (2015) 265–271, <https://doi.org/10.1016/j.solener.2015.04.010>.
- [15] B. Hallam, A. Urueña, R. Russell, M. Aleman, M. Abbott, C. Dang, et al., Efficiency enhancement of i-PERC solar cells by implementation of a laser doped selective emitter, *Sol. Energy Mater. Sol. Cells* 134 (2015) 89–98, <https://doi.org/10.1016/j.solmat.2014.11.028>.
- [16] U. Jäger, M. Okanovic, M. Hörtelis, A. Grohe, R. Preu, Selective emitter by laser doping from phosphosilicate glass, in: Proceedings of the 24th European Photovoltaic Solar Energy Conference, 2009, pp. 1740–1743, <https://doi.org/10.4229/24thEUPVSEC2009-2CV.5.9>.
- [17] A. Dastgheib-Shirazi, M. Steyer, G. Micard, H. Wagner, P.P. Altermatt, G. Hahn, Relationships between diffusion parameters and phosphorus precipitation during the POCl_3 diffusion process, *Energy Proc.* 38 (2013) 254–262, <https://doi.org/10.1016/j.egypro.2013.07.275>.
- [18] S. Werner, S. Mourad, W. Hasan, A. Wolf, Structure and composition of phosphosilicate glass systems formed by POCl_3 diffusion, *Energy Proc.* 124 (2017) 455–463, <https://doi.org/10.1016/j.egypro.2017.09.280>.
- [19] M. Kim, D. Kim, D. Kim, Y. Kang, Influence of laser damage on the performance of selective emitter solar cell fabricated using laser doping process, *Sol. Energy Mater. Sol. Cells* 132 (2015) 215–220, <https://doi.org/10.1016/j.solmat.2014.08.021>.
- [20] G. Heinrich, M. Bähr, K. Stolberg, T. Wütherich, M. Leonhardt, A. Lawerenz, Investigation of ablation mechanisms for selective laser ablation of silicon nitride layers, *Energy Proc.* 8 (2011) 592–597, <https://doi.org/10.1016/j.egypro.2011.06.188>.
- [21] T. Fellmeth, A. Born, A. Kimmerle, F. Clement, D. Biro, R. Preu, Recombination at metal-emitter interfaces of front contact technologies for highly efficient silicon solar cells, *Energy Proc.* 8 (2011) 115–121, <https://doi.org/10.1016/j.egypro.2011.06.111>.
- [22] S. Narasimha, A. Rohatgi, Effective passivation of the low resistivity silicon surface by a rapid thermal oxide/plasma silicon nitride stack, *Appl. Phys. Lett.* 72 (1998) 1872–1874, <https://doi.org/10.1063/1.121211>.
- [23] C.P. Liu, M.W. Chang, C.L. Chuang, Effect of rapid thermal oxidation on structure and photoelectronic properties of silicon oxide in monocrystalline silicon solar cells, *Curr. Appl. Phys.* 14 (2014) 653–658, <https://doi.org/10.1016/j.cap.2014.02.017>.
- [24] S.S. Liao, C.L. Chuang, Y.C. Lin, C.F. Dee, B.Y. Majlis, E.Y. Chang, Effect of surface passivation by a low pressure and temperature environment-grown thermal oxide layer for multi-crystalline silicon solar cells, *Thin Solid Films* 660 (2018) 1–9, <https://doi.org/10.1016/j.tsf.2018.05.047>.
- [25] N.C. Mandal, S. Biswas, S. Acharya, T. Panda, S. Sadhukhan, J.R. Sharma, et al., Study of the properties of SiO_x layers prepared by different techniques for rear side passivation in TOPCon solar cells, *Mater. Sci. Semicond. Process.* 119 (2020) 105163, <https://doi.org/10.1016/j.mssp.2020.105163>.
- [26] C. Liu, D. Chen, Y. Chen, Y. Ling, Y. Zou, Y. Wang, et al., Industrial TOPCon solar cells on n-type quasi-mono Si wafers with efficiencies above 23%, *Sol. Energy Mater. Sol. Cells* 215 (2020), 110690, <https://doi.org/10.1016/j.solmat.2020.110690>.
- [27] A. Oates, H.S. Reehal, Effect of diffusion parameters on emitter formation in silicon solar cells by proximity rapid thermal diffusion, *Mater. Sci. Semicond. Process.* 77 (2018) 83–87, <https://doi.org/10.1016/j.mssp.2017.12.006>.
- [28] M. Cui, C. Jin, L. Zhuge, X. Wu, The impact of diffusion gettering on solar cell efficiency and light induced degradation, *Optik* 181 (2019) 129–133, <https://doi.org/10.1016/j.ijleo.2018.12.021>.
- [29] W. Lin, D. Chen, C. Liu, Y. Wang, Y. He, Y. Zou, et al., Green-laser-doped selective emitters with separate BBr_3 diffusion processes for high-efficiency n-type silicon solar cells, *Sol. Energy Mater. Sol. Cells* 210 (2020), 110462, <https://doi.org/10.1016/j.solmat.2020.110462>.
- [30] M. Stavola, F. Jiang, S. Kleekajai, L.L. Wen, C. Peng, V. Yelundur, et al., Hydrogen passivation of defects in crystalline silicon solar cells, *Mater. Res. Soc. Symp. Proc.* 1210 (2010) 3–13, <https://doi.org/10.1557/PROC-1210-Q01-01>.
- [31] H. Li, B. Hallam, S. Wenham, M. Abbott, Oxidation drive-in to improve industrial emitter performance by POCl_3 diffusion, *IEEE J. Photovoltaics* 7 (2017) 144–152, <https://doi.org/10.1109/jphotov.2016.2631300>.
- [32] J. Häkkinen, V.P. Lempinen, T. Juvinen, J. Kyllmäläuma, Recovery of minority carrier lifetime in low-cost multicrystalline silicon, *Sol. Energy Mater. Sol. Cells* 73 (2002) 125–130, [https://doi.org/10.1016/S0927-0248\(01\)00117-9](https://doi.org/10.1016/S0927-0248(01)00117-9).
- [33] M.G. Burzo, P.L. Komarov, P.E. Raad, Thermal transport properties of gold-covered thin-film silicon dioxide, *IEEE Trans. Compon. Packag. Technol.* 26 (2003) 80–88, <https://doi.org/10.1109/TCAPT.2003.811467>.
- [34] A. Delan, M. Rennau, S.E. Schulz, T. Gessner, Thermal conductivity of ultra low-k dielectrics, *Microelectron. Eng.* 70 (2003) 280–284, [https://doi.org/10.1016/S0167-9317\(03\)00417-9](https://doi.org/10.1016/S0167-9317(03)00417-9).
- [35] X. Gu, S. Li, H. Bao, Thermal conductivity of silicon at elevated temperature: role of four-phonon scattering and electronic heat conduction, *Int. J. Heat Mass Tran.* 160 (2020), 120165, <https://doi.org/10.1016/j.ijheatmasstransfer.2020.120165>.
- [36] H.P. Yin, K. Tang, J.B. Zhang, W. Shan, X.M. Huang, X.D. Shen, Bifacial n-type silicon solar cells with selective front surface field and rear emitter, *Sol. Energy Mater. Sol. Cells* 208 (2020), 110345, <https://doi.org/10.1016/j.solmat.2019.110345>.
- [37] E. Kobayashi, S.D. Wolf, J. Levrat, A. Descoedres, M. Despeisse, F.J. Haug, et al., Increasing the efficiency of silicon heterojunction solar cells and modules by light soaking, *Sol. Energy Mater. Sol. Cells* 173 (2017) 43–49, <https://doi.org/10.1016/j.solmat.2017.06.023>.
- [38] M. Nicolai, M. Zanuccoli, M. Galiazzo, M. Bertazzo, E. Sangiorgi, C. Fiegna, Simulation study of light-induced, current-induced degradation and recovery on PERC solar cells, *Energy Proc.* 92 (2016) 153–159, <https://doi.org/10.1016/j.egypro.2016.07.014>.